Theoretical and Applied Fracture Mechanics 125 (2023) 103838

Contents lists available at ScienceDirect

Theoretical and Applied Fracture Mechanics

journal homepage: www.elsevier.com/locate/tafmec

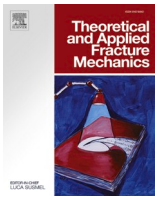

Study of the influence of current density and displacement rate on hydrogen embrittlement using small punch tests

G. Álvarez *, V. Arniella, F.J. Belzunce, C. Rodríguez

SIMUMECAMAT Research Group, Polytechnic Engineering School, University of Oviedo, Gijón 33203, Spain

ARTICLE INFO

Keywords:
Hydrogen embrittlement
SPT
In-situ hydrogen charged tests
Electrochemical charging

ABSTRACT

Susceptibility to hydrogen embrittlement was studied on quenched and tempered 42CrMo steel with Small Punch Tests (SPT) using different punch displacement rates. Hydrogen was cathodically charged using an electrolyte composed of 1 M H_2SO_4 with 0.25 g/l As_2O_3, and two different cathodic current densities (0.50 and 1.00 mA/cm^2). The results were analysed using different embrittlement indices: related to the energy consumed at maximum load, to the equivalent biaxial deformation at failure location and to the failed diameter. Failure location is directly related to punch displacement and, consequently, to embrittlement.

All embrittlement indices increase as the punch displacement rate decreases (longer time for hydrogen diffusion) and as the cathodic current density increases (higher hydrogen concentration in equilibrium with the hydrogenated medium). On the other hand, the use of a pre-charging time before the start of the in-situ hydrogen charged test produces no change in the results, as most hydrogen enters the sample due to the high plastic deformation induced on its surface in the course of the mechanical test.

1. Introduction

The importance of hydrogen as an energy vector is now widely recognized by both the scientific community and the general public. Hydrogen energy technology is being developed to reduce the emission of CO_2 to the atmosphere and to decrease climate change evolution. The current demand for hydrogen is triple that in 1975 [1], thus there is a special interest in safe transport and storage of this element. Steel is the most suitable material to manufacture pressure vessels and pipelines to transport hydrogen. Austenitic stainless steel is the most reliable grade, but its high price and low yield strength are drawbacks. It is necessary to consider the suitability of other types of steels that combine high mechanical strength and good behaviour in the presence of this gas, minimizing hydrogen embrittlement, HE [2-5].

To evaluate the mechanical properties of materials in the face of this phenomenon, it is necessary to use specific equipment and procedures. Different research works have used standard tests such as tensile tests [6,7], slow strain rate testing [8-10], fracture toughness [11-13], and crack growth fatigue resistance tests [14-16]. These techniques are the most used because of their extended use in the mechanical characterization of materials under standard conditions. However, these tests require samples with large dimensions; if the sample does not have enough material, it is difficult to characterize specific components and structures. This is the case with welded joints or very low thickness components. For these cases, miniature tests have been developed over the last decades [17-19]. Most of these techniques have yet to be standardized, but they can help to evaluate the modification of certain mechanical properties in well-defined environments. One of the most widely used miniature tests is the Small Punch Test (SPT), which is used to evaluate the tensile and fracture properties of materials in laboratory conditions when only a small amount of material is available [20]. It can be used to evaluate the mechanical behaviour of different kind of materials [21,22], particularly metallic materials [23-25], for which test standards have been developed in both the USA and Europe [26,27].

Various researchers have also used SPT to study the effect of the external environment on the mechanical properties of steels [28-30]. Some of them have applied this methodology to characterize hydrogen embrittlement phenomena, but with different boundary conditions and therefore, different results [31,32].

It has been found that the presence of internal hydrogen (pre-charged before the SPT execution) does not always affect the mechanical behaviour of these small specimens, especially when the amount of hydrogen is low [18] or the test displacement rate is fast [33]. The reason for this behaviour is the egress of the pre-charged hydrogen from

* Corresponding author.
E-mail address: alvarezdguillermo@uniovi.es (G. Álvarez).

https://doi.org/10.1016/j.tafmec.2023.103838
Received 28 November 2022; Received in revised form 28 February 2023; Accepted 28 February 2023
Available online 4 March 2023

the specimen in the course of the mechanical test [34].

On the other hand, the use of SP tests with in-situ hydrogen charging, where the entry of hydrogen occurs during the mechanical test, has provided better results [17]. However, there are still many open questions. Firstly, the way in which hydrogen is introduced into the sample: from a gaseous atmosphere or electrochemically [35-38]. The use of a pressurized hydrogen gas atmosphere would seem to be the most appropriate method given that these are the in-service conditions in most cases. Nevertheless, in addition to being a more expensive method, the applied pressure can affect the standard SPT results. Hydrogen electrolytic charge does not have, however, any of these handicaps, and test conditions would be representative of the in-service ones if the same amount of internal hydrogen were guaranteed. For this, it is necessary to analyse not only how the electrolytic charging parameters (mainly current density) affect the hydrogen concentration, but also the deformation rate (punch displacement rate) applied during the test. It is known that the rate of hydrogen ingress into the sample grows with the strain rate [39]. Therefore, the longer the time at a given deformation (lower test rates), the greater the amount of hydrogen entering the specimen.

In order to clarify the above questions, the SPT methodology under in-situ electrochemical hydrogen charging conditions was used in this work to analyse the susceptibility to HE of a quenched and tempered 42CrMo4 steel. Two different current densities (0.50 mA/cm^2 and 1.00 mA/cm^2) were used for electrochemical charging to generate different hydrogen boundary conditions and hydrogen concentrations similar to real in-service industrial conditions. The SPT tests were performed at various displacement rates, obtaining different local hydrogen concentrations. The influence of different hydrogen pre-charging times prior to in-situ SPT mechanical tests was also evaluated in this research.

2. Materials and experimental procedure

2.1. Materials

The material used in this study was a commercial 42CrMo4 steel whose chemical composition is shown in Table 1. It is a medium carbon steel alloyed with Cr and Mo. The good combination of strength and toughness, in addition to its high fatigue resistance, make this steel an ideal candidate for use in high-pressure hydrogen environments.

A plate of this steel (250x250x12 mm) was submitted to a heat treatment consisting of austenitizing at 845 °C for 40 min, followed by quenching in room temperature water and finally tempering at 700 °C for 2 h. Fig. 1 shows the microstructure of the steel. It is tempered martensite, in which carbide precipitation during the tempering stage is notorious. As a relatively high tempering temperature was applied (700 °C), internal stresses induced in the quench stage were relaxed and carbides precipitated and grew to attain a uniform distribution with a quasi-globular shape (SEM image in Fig. 1.a). Most crystallographic orientations are present in the EBSD image shown in Fig. 1.b). This treatment was selected after an intensive study carried out by A. Zafra et al. [40,41].

This steel was characterized in a previous work [39] using tensile and fracture toughness tests according to the UNE-EN-10002–1 [42] and ASTM E1820 [43] respectively. The measured hardness (HV10), yield stress (σ_{YS}), ultimate tensile strength (σ_U), tensile elongation (e), reduction of area (RA) and fracture toughness (J_{Ic}) are shown in Table 2.

Table 1
Chemical composition of 42CrMo4 steel (% weight).

Material	C	Cr	Mo	Mn	Si	P	S
42CrMo4	0.42	0.98	0.22	0.62	0.18	0.008	0.002

2.2. Hydrogen charging method

To simulate the working conditions for structures and components in the presence of hydrogen, an electrochemical hydrogen charging method was used. The electrolyte was 1 M H_2SO_4 + 0.25 g/l As_2O_3, as it had been used successfully in previous research works [41,44].

According to V. Arniella et al. [45] using this electrolyte and 0.50 mA/cm^2 of current density, we can obtain an homogenous hydrogen distribution inside a cylinder 5 mm in diameter and 30 mm in length after 3 h of charging time. Furthermore, in order to increase hydrogen ingress in the sample, the same charging conditions but with a higher current density (1.00 mA/cm^2) was also used by the aforementioned authors [45]. Table 3 shows the hydrogen concentrations at saturation (3 h) obtained using both current densities.

Hydrogen diffusivity in the steel was analysed using electrochemical permeation tests. The applied experimental set up was explained by G. Álvarez et al. [12]. In order to assess whether the hydrogen diffusion coefficient depends on the current density, permeation tests were performed applying cathodic current densities of 0.50 and 1.00 mA/cm^2 in the permeation cell. The obtained results, recovered in Fig. 2, show how the transient varies with the applied cathodic current density, but the diffusion coefficient is quite similar under both conditions: 2.89 10^{-10} m^2/s and 4.27 10^{-10} m^2/s, for 0.50 mA/cm^2 and 1.00 mA/cm^2, respectively. Based on these results, it can be assumed that the use of a current density of 0.50 or 1.00 mA/cm^2 will influence the hydrogen concentration inside the sample but its effect on the diffusivity of the steel will be negligible. Thus, an average hydrogen diffusion coefficient of 3.58 10^{-10} m^2/s was used in the rest of the paper.

2.3. Small punch tests

Small punch tests (SPT) were carried out using a standard SPT device [46] with slight modifications to facilitate hydrogen entrance into the sample surface from the previously described electrolyte while the mechanical test is carried out (in-situ hydrogen charged SPT). The standard SPT device has a matrix die hole with a diameter of 4 mm and uses a hemispherical-head punch 2.5 mm in diameter. To carry out the in-situ electrochemically hydrogen charged SPT, the matrix die was placed at the top and the punch at the bottom of the assembly (Fig. 3.a) and the electrolyte was introduced in the small internal chamber machined just above the matrix die, where a Pt electrode was also placed. A cathodic current density (0.50 or 1.00 mA/cm^2) was applied using a Pt counterelectrode. All parts of the device in contact with the electrolyte were made of ceramic material (Al_2O_3) to avoid electric current losses.

Square SPT specimens with nominal dimensions of 10x10x0.5 mm were used. The load was applied using a mechanical testing machine equipped with a 5 kN-capacity load cell and the punch displacement was measured with a COD extensometer. All the tests were performed in laboratory conditions of pressure and temperature (1 bar, 25 °C). Nevertheless, in order to evaluate the effect of the test displacement rate, punch displacement rates varying from 0.001 mm/min to 0.26 mm/min were used in the in-situ SP tests. The results obtained from these tests were compared with those obtained from specimens tested without hydrogen using a standard test rate of 0.20 mm/min [25]. At least two SPT specimens were tested under each condition.

To determine whether pre-charging previous to the in-situ SP test influences the results, some in-situ SPTs were performed using hydrogen pre-charged specimens. To establish the necessary pre-charging time for this specimen geometry (0.5 mm thickness) a diffusion finite element model described in A. Zafra et al [41] was used. Considering the diffusion coefficient obtained for both current densities, pre-charge times of 7 min (1.00 mA/cm^2) and 15 min (0.50 mA/cm^2) were calculated to saturate the sample. Based on these results a pre-charging time of 15 min was used for both current densities.

To quantify the embrittlement of hydrogen, the SPT Hydrogen Embrittlement Index, HEI_{X_SPT}, defined in equation (2) was used:

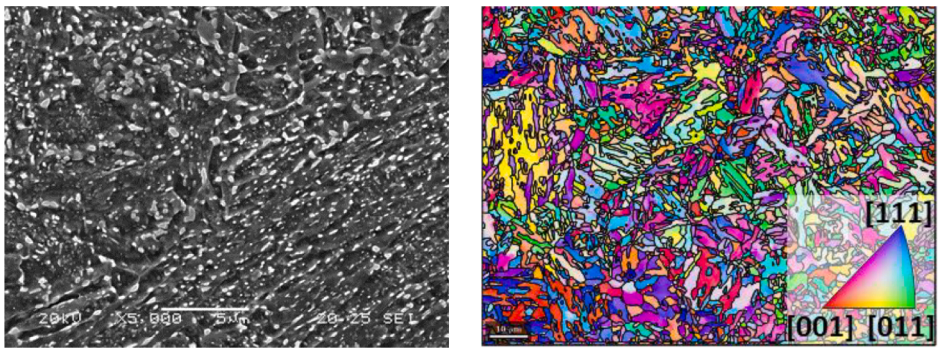

(a) (b)

Fig. 1. SEM-EBSD images of the heat treated 42CrMo4 steel, (a) SEM; (b) EBSD.

Table 2
Mechanical properties of the steel.

Material	Hardness (HV10)	σ_y (MPa)	σ_u (MPa)	e (%)	RA (%)	J_{Ic} (kJ/m^2)
42CrMo4	207	622	710	22	61	580

Table 3
Hydrogen concentration measurements under different current densities in the 42CrMo4 steel, [45].

Electrolyte	Current density (mA/cm^2)	Hydrogen concentration, C_0 (ppm)
1 M H_2SO_4 + 0.25 g/l As_2O_3	0.50	0.90 ± 0.1
	1.00	1.20 ± 0.1

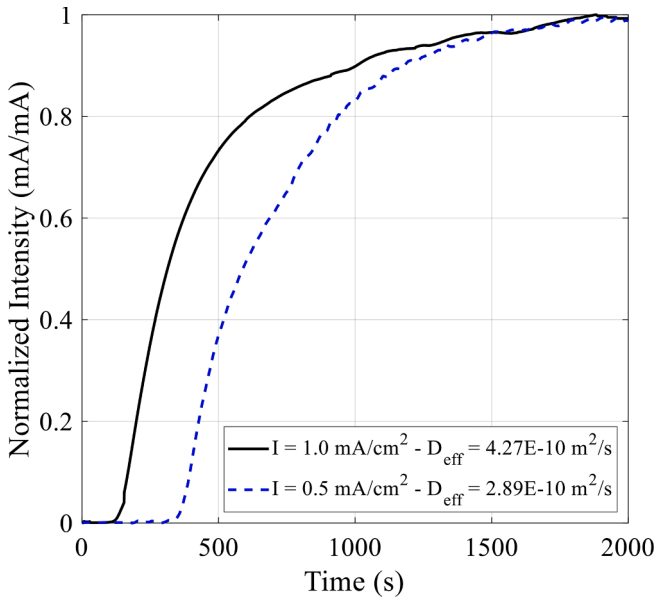

Fig. 2. Permeation test results: normalized intensity (permeation current density over steady state current density) versus permeation time.

$$HEI_X(\%) = \frac{X_{SPT}^{Air} - X_{SPT}^{Hydrogen}}{X_{SPT}^{Air}} \times 100 \quad (2)$$

where X_{SPT}^{Air} and $X_{SPT}^{Hydrogen}$ represent the value of an appropriate SPT parameter measured in air and under in-situ hydrogen charging respectively. One of the most used parameter to be used in equation (2) is the *SPT fracture energy*, W_{SPT} [18]. It is defined as the area under the SPT curve up to the maximum load (W_{SPT}, Fig. 3.b) divided by the square of the specimen thickness. The HEI_{WSPT} could be expressed by equation (3):

$$HEI_{WSPT}(\%) = \frac{W_{SPT}^{Air}/t_0^2 - W_{SPT}^{Hydrogen}/t_0^2}{W_{SPT}^{Air}/t_0^2} \times 100 \quad (3)$$

Another SPT parameter that could be used to express brittleness caused by hydrogen is the *equivalent biaxial deformation at failure*, ε_{qf}, which is a parameter directly linked with the fracture toughness of steels [25,47]. Expression (4) was used to calculate the ε_{qf}, where t_f is the local thickness at the failure location and t_0 is the initial thickness of the SPT sample (see Fig. 4):

$$\varepsilon_{qf} = \ln\left(\frac{t_0}{t_f}\right) \quad (4)$$

Therefore, $HEI_{\varepsilon qf}$ defines the hydrogen embrittlement index when ε_{qf} is the X parameter in equation (2). To measure the final local thickness of the failed zone, t_f, the specimen was diametrically cut as shown in Fig. 4 for ductile (Fig. 4.a) and brittle (Fig. 4.b) behaviours. When ductile failure occurs, a semi-circular crack develops in the failed region of the sample (smile-shaped failure) [25]. On the other hand, brittle failure gives rise to a circular crack with additional radial cracks [31]. As both failure patterns can be fitted by a circle of diameter ϕ this *failure diameter* could be another appropriate parameter to estimate the hydrogen embrittlement index, HEI_ϕ. A scanning electron microscope (SEM JEOL-JSM5600) was used to accurately measure both, failure thickness and failure diameter of the tested SPT specimens.

3. Results

3.1. Influence of hydrogen pre-charging

Fig. 5 shows the load-punch displacement curves obtained when the in-situ hydrogen charging SP test was carried out at the standard test rate (0.20 mm/min) with and without previous hydrogen pre-charging (15 min of hydrogen pre-charging). This figure also shows, as a comparison, the SPT curves obtained with the material tested in air (without H charging). Table 4 resumes the corresponding SPT parameters (mean ± standard deviation).

Under in-situ hydrogen charging, hydrogen embrittlement was detected by a decrease in the maximum load, P_m, and punch displacement, d_m, and, consequently, in the fracture energy, W_{SPT}, even at the standard test rate of 0.20 mm/min. This embrittlement increases when the largest cathodic current density of 1.00 mA/cm^2 was applied. The greater the applied cathodic current density, the greater the hydrogen concentration at the specimen surface (Table 3), thus, embrittlement is increased.

On the contrary, the use of a pre-charging time of 15 min before the

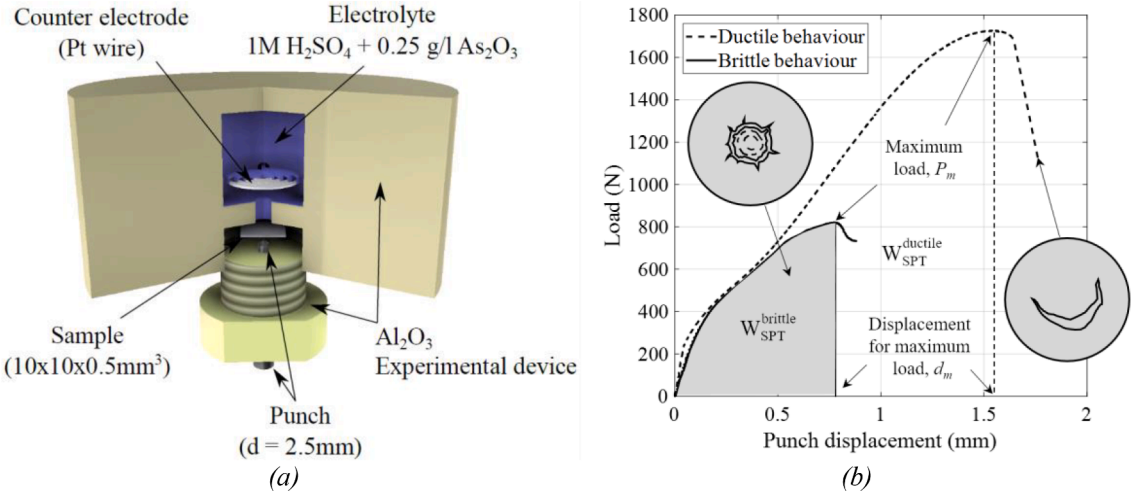

Fig. 3. SPT testing procedure. (a) SPT device; (b) Load-Punch displacement curves.

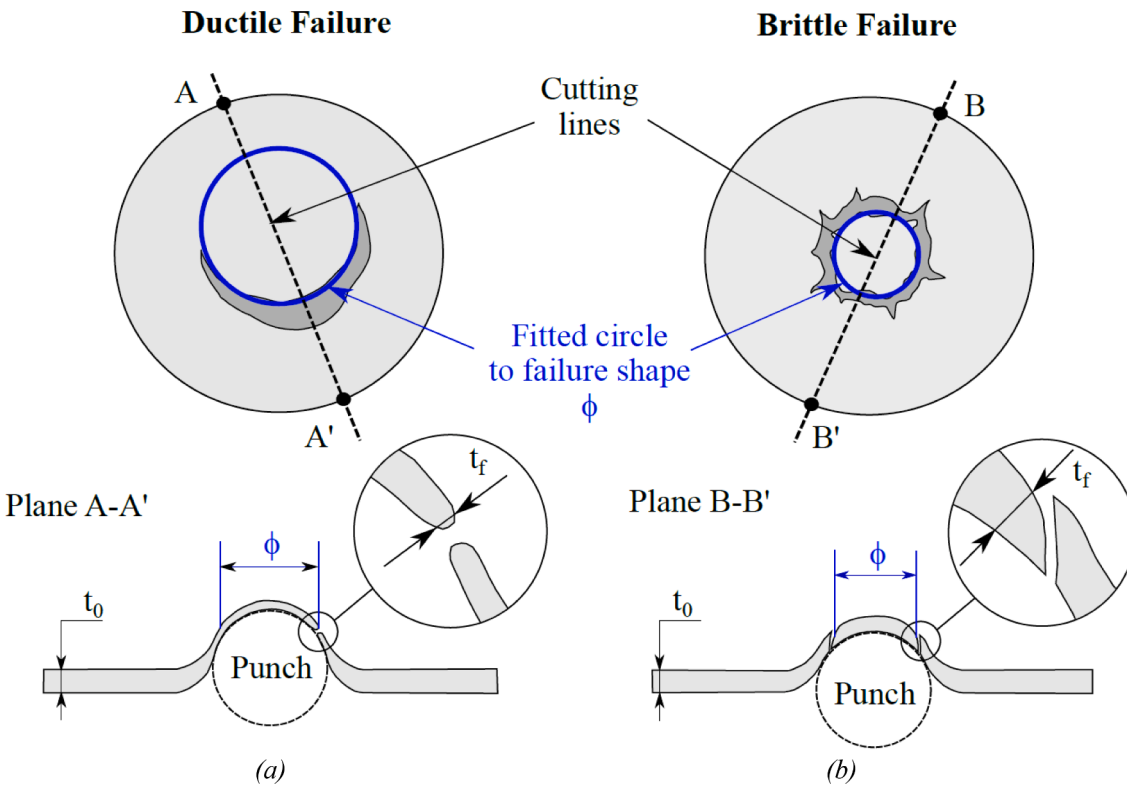

Fig. 4. SPT failure shape and thickness reduction in (a) ductile failure; (b) brittle failure.

start of the in-situ SPTs does not affect embrittlement: similar SPT parameters were obtained with and without pre-charging. During the SPT, the largest tensile stress occurs on the sample surface, where hydrogen is entering the specimen and the corresponding hydrogen content in equilibrium with the cathodic current density is attained very quickly. On the other hand, a lower hydrogen content is introduced during pre-charging (no mechanical load is applied) than during the in-situ hydrogen charged test, where high plastic deformation is generated on the sample surface. Zafra et al [39] measured a four-fold increase in hydrogen concentration in 42CrMo4 steel when a plastic pre-deformation of 50% was applied.

3.2. Influence of displacement rate and current density in the in-situ hydrogen charged tests

Fig. 6 shows the SPT curves obtained in the in-situ hydrogen charged tests using different displacement rates under cathodic current densities of 0.50 mA/cm^2 (Fig. 6.a) and 1.00 mA/cm^2 (Fig. 6.b). Taking into account that hydrogen pre-charging does not influence the mechanical behaviour observed in these tests, this analysis was performed without pre-charging the specimens. Punch displacement rates were varied between 0.001 and 0.26 mm/min.

As can be seen in Fig. 6 and Table 5, regardless of the applied cathodic current density, as the displacement rate decreases so do the values of the maximum load, P_m, and the displacement at maximum load, d_m. Consequently, the fracture SPT energy, W_{SPT}, also decreases.

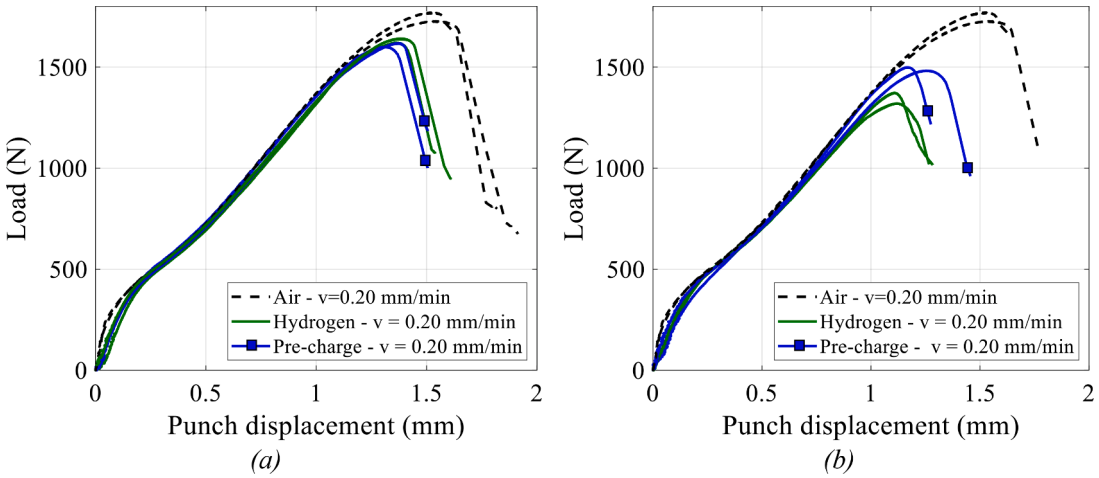

Fig. 5. SPT curves in air, under in-situ hydrogen charging and with additional hydrogen pre-charging (a) 0.50 mA/cm^2; (b) 1.00 mA/cm^2. Punch displacement rate: 0.20 mm/min.

Table 4
SPT results for uncharged, under in-situ H-charging and under in-situ H-charged with 15 min of H-pre-charging. Punch displacement rate: 0.20 mm/min.

Test condition	i_c (mA/cm^2)	t_0 (mm)	P_m (N)	d_m (mm)	W/t_0^2 (N/mm)
Air	–	0.466 ± 0.006	1764 ± 31	1.54 ± 0.04	7442 ± 392
In-situ H-charged without pre-charging	0.50	0.471 ± 0.001	1630 ± 14	1.37 ± 0.01	5965 ± 431
	1.00	0.487 ± 0.011	1346 ± 37	1.11 ± 0.01	3647 ± 174
In-situ H charged (with pre-charging	0.50	0.473 ± 0.009	1609 ± 13	1.34 ± 0.04	5622 ± 355
	1.00	0.482 ± 0.013	1499 ± 12	1.17 ± 0.06	4350 ± 515

Comparing the results obtained under the two applied cathodic current densities, it is clear that hydrogen embrittlement increases slightly under a larger cathodic current density, although this effect is barely appreciated under the lowest displacement rates.

3.3. Post-failure analysis

Images of the in-situ hydrogen charged specimens after failure are included in Figs. 7 and 8. These figures show cross-sections (above) and top views (below) of the failed specimens tested under the different displacement rates at 0.50 mA/cm^2 (Fig. 7) and 1.0 mA/cm^2 (Fig. 8) cathodic current densities. Mean ± Standard Deviation values of final thickness at the failed region (t_f), equivalent biaxial deformation at failure (ε_{qf}) and the corresponding diameter of the circle fitted to the failed zone (ϕ) are shown in Table 6.

Images presented in Figs. 7 and 8 show a clear decrease in the deformation of the specimens as well as a decrease of the thickness of the failed region (t_f) as the applied displacement rate decreases and the cathodic current density increases. Consequently, as can be seen in Table 6, the equivalent biaxial deformation at failure (ε_{qf}) also decreases under lower displacement rates and higher cathodic current density.

Images shown in the lower rows of Figs. 7 and 8 also evidence the decrease in the diameter of the failed zone (ϕ) with the decreasing of the displacement rate and higher cathodic current density. The presence of radial cracks in the failed region of the specimens also denotes hydrogen embrittlement. As the test rate decreases or cathodic current density increases, more radial cracks appear on the surface of these specimens (Figs. 7 and 8).

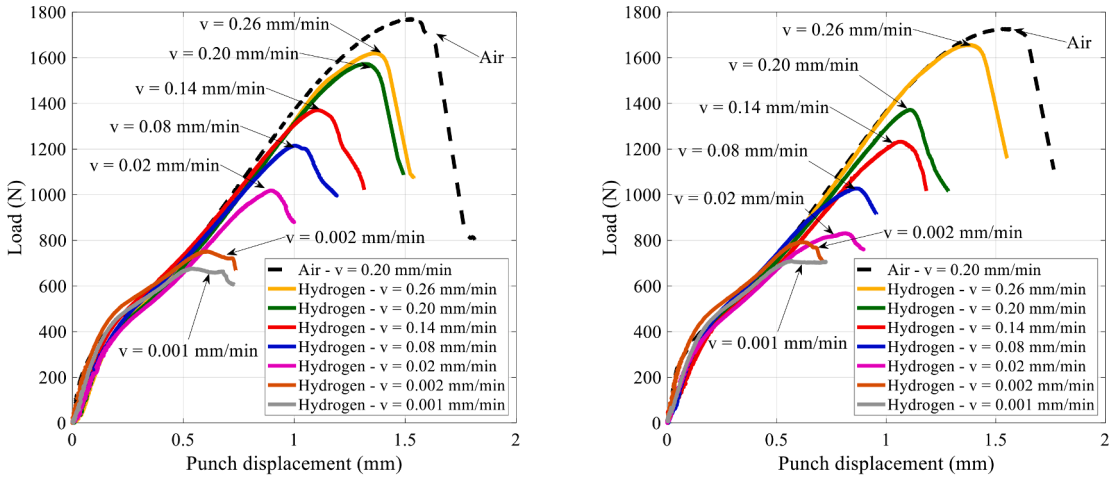

Fig. 6. SPT curves at current densities of (a) 0.50 mA/cm^2 and (b) 1.00 mA/cm^2.

Table 5
SPT results for different displacement rates and cathodic current densities.

Test condition	i_c (mA/cm^2)	v (mm/min)	t_0 (mm)	P_m (N)	d_m (mm)	*testing time* (min)	W/t_0^2 (N/mm)
Air	–	0.20	0.466 ± 0.006	1764 ± 31	1.54 ± 0.04	10.8 ± 0.1	7442 ± 392
In situ	0.50	0.26	0.476 ± 0.011	1600 ± 38	1.30 ± 0.03	7.8 ± 1.5	5965 ± 602
		0.20	0.471 ± 0.001	1630 ± 14	1.37 ± 0.01	9.4 ± 0.6	5422 ± 431
		0.14	0.486 ± 0.002	1418 ± 66	1.12 ± 0.02	11.8 ± 1.3	3919 ± 171
		0.08	0.479 ± 0.008	1211 ± 29	1.00 ± 0.03	17.3 ± 0.3	3133 ± 53
		0.02	0.461 ± 0.010	1015 ± 62	0.91 ± 0.03	66.8 ± 2.2	2636 ± 242
		0.002	0.460 ± 0.005	709 ± 90	0.61 ± 0.02	435.6 ± 17.0	1516 ± 381
		0.001	0.477 ± 0.001	582 ± 51	0.57 ± 0.04	799.2 ± 66.0	1101 ± 136
	1.00	0.26	0.478 ± 0.013	1616 ± 59	1.35 ± 0.01	7.4 ± 0.2	5577 ± 794
		0.20	0.487 ± 0.011	1346 ± 37	1.11 ± 0.01	7.6 ± 0.1	3647 ± 174
		0.14	0.476 ± 0.009	1362 ± 52	1.12 ± 0.01	10.8 ± 0.6	3529 ± 68
		0.08	0.491 ± 0.012	1078 ± 97	0.91 ± 0.08	15.6 ± 1.7	2508 ± 383
		0.02	0.455 ± 0.002	826 ± 7	0.80 ± 0.03	54.9 ± 0.4	2147 ± 96
		0.002	0.461 ± 0.006	639 ± 32	0.62 ± 0.01	416.7 ± 14.1	1361 ± 36
		0.001	0.481 ± 0.006	683 ± 90	0.57 ± 0.04	780.5 ± 42.4	1135 ± 23

4. Discussion

Expression (2) quantifies the susceptibility to hydrogen embrittlement under the different testing conditions using the appropriate SPT parameter. Table 7 shows the hydrogen embrittlement indices obtained using the *fracture SPT energy (HEI_{WSPT}), the equivalent biaxial deformation ($HEI_{\varepsilon qf}$)*, and *the diameter at failure (HEI_{ϕ})*. These HEI values plotted versus the punch displacement rate are shown in Fig. 9.

As can be seen, for a given current density and regardless of the embrittlement index used, the susceptibility of the steel to hydrogen embrittlement increases as the applied test rate decreases up to a certain threshold. For the steel and hydrogen charging conditions used in this work, maximum embrittlement is achieved when the test rate is approximately 0.002 mm/min. As can be seen in Fig. 9, with a higher cathodic current density, the obtained embrittlement indices are always slightly higher.

In the in-situ hydrogen charging SPTs, the steel is affected by hydrogen even when the highest punch displacement rate is used, with HEI_{WSPT} (see Fig. 9.a) between 20% (i_c = 0.50 mA/cm^2) and 25% (i_c = 1.00 mA/cm^2), and even 30% (i_c = 0.50 mA/cm^2) and 42% (i_c = 1.00 mA/cm^2) when $HEI_{\varepsilon qf}$ is used (Fig. 9.b).

These embrittlement values show a three-fold increase when a test rate 10 times slower is applied (v = 0.02 mm/min), but do not continue growing as fast when the test rate decreases 10 times more (v = 0.002 mm/min) and the embrittlement growth is barely appreciated when the displacement test rate decreases to 0.001 mm/min. The HEI_{ϕ} index shows lower embrittlement values but a similar trend than the HEI_{WSPT} and $HEI_{\varepsilon qf}$.

The evolution of all the HE indices with the test displacement rate is very similar. All indices show a decreasing dependence on the punch displacement rate as this parameter drops, but finally tend towards a nearly constant value when the critical displacement rate of 0.002 mm/min is reached. Based on these results and given the similar behaviour observed with the different embrittlement indices, all of them are considered valid to quantify the effect of the presence of hydrogen on the mechanical behaviour of the analysed steel.

Furthermore, and regardless of the *HEI* used, Fig. 9 shows the importance of hydrogen charging conditions. First at all, the steel is sensitive to the presence of hydrogen in the in-situ hydrogen charged tests even under the fast test displacement rate recommended by the standard, which is not true when the SPT tests are performed on hydrogen pre-charged specimens (ex-situ tests) [18]. Hydrogen losses on the hydrogen pre-charged specimens during test preparation and running undoubtedly explain this behaviour. Secondly, hydrogen embrittlement increases as the test displacement rate decreases and when cathodic current density grows. As the displacement rate decreases, testing time increases, giving more time for hydrogen diffusion from the surface of the sample to interior. This process continues until a sufficiently low displacement rate is applied and hydrogen saturation is attained in the whole sample. On the other hand, when a larger cathodic current density is applied, a higher hydrogen content in equilibrium with the electrolyte is generated on the sample surface. This gives rise to higher hydrogen gradients in the sample and, consequently, to larger embrittlement indices. Moreover, local surface plastic deformation while hydrogen is entering in the sample in the course of the in-situ hydrogen charged SP tests induces much higher hydrogen concentration than when tests are performed in air on pre-charged samples.

Fig. 10 shows the evolution of the SPT curves obtained in air and with in-situ hydrogen charging (Fig. 10.a) as well as the location of the most stressed regions (Fig. 10.b and c) in these tests. According to [48], the location of maximum stresses in an SPT specimen changes continuously during the test due to punch friction and to specimen thickness

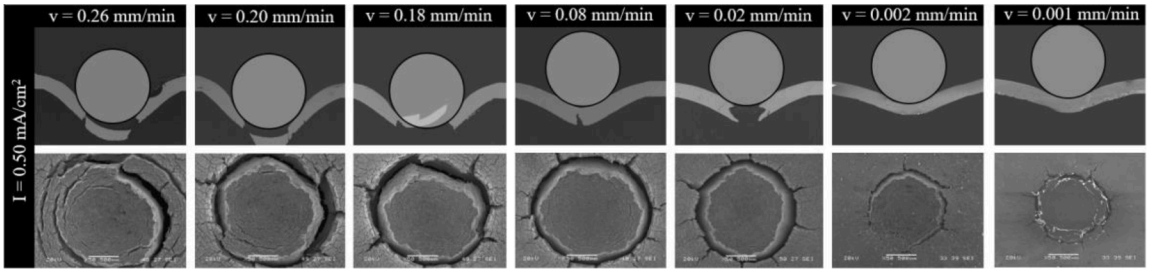

Fig. 7. In-situ SPTs post-failure images corresponding to samples tested under an applied current density of 0.5 mA/cm^2.

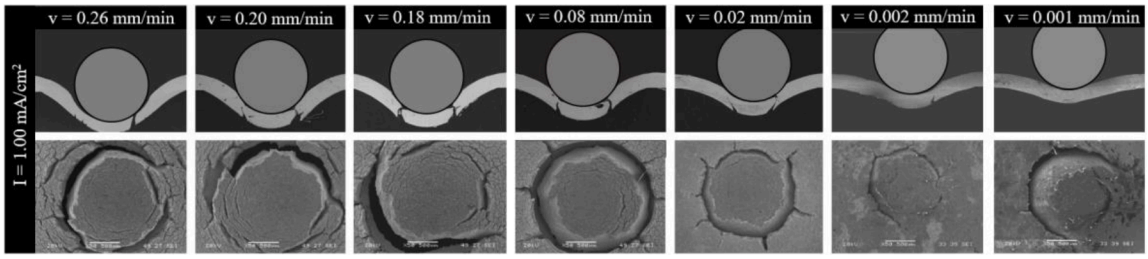

Fig. 8. In-situ *SPTs post-failure images corresponding to samples tested under an applied current density of 1.0 mA/cm².*

Table 6
Post-failed SPT measurements in tests performed under different displacement rates and current densities.

Test condition	i_c (mA/cm^2)	v (mm/min)	t_f (mm)	ε_{qf} (-)	ϕ (mm)
Air	–	0.20	0.158	1.08	1.89
In situ	0.50	0.26	0.224	0.76	1.62
		0.20	0.254	0.62	1.59
		0.14	0.316	0.43	1.55
		0.08	0.392	0.16	1.43
		0.02	0.479	0.06	1.21
		0.002	0.356	0.11	1.11
		0.001	0.406	0.07	1.03
	1.00	0.26	0.258	0.62	1.58
		0.20	0.346	0.34	1.55
		0.14	0.376	0.24	1.49
		0.08	0.393	0.22	1.38
		0.02	0.423	0.05	1.17
		0.002	0.408	0.05	1.06
		0.001	0.396	0.08	1.05

Table 7
Hydrogen embrittlement results.

I (mA/cm^2)	v (mm/min)	HEI_{WSPT} (%)	$HEI_{\varepsilon qf}$ (%)	HEI_{ϕ} (%)
0.50	0.26	19.85	30.01	14.29
	0.20	27.14	42.88	15.71
	0.14	47.34	60.07	17.99
	0.08	57.90	85.17	24.53
	0.02	64.58	94.44	35.98
	0.002	79.63	90.04	41.32
	0.001	85.21	93.52	45.50
1.00	0.26	25.07	42.88	16.32
	0.20	51.00	68.25	17.99
	0.14	52.58	78.15	21.16
	0.08	66.30	79.32	26.68
	0.02	71.15	95.37	38.10
	0.002	81.71	95.44	43.92
	0.001	84.75	92.60	44.29

reduction. Taking the centre of the specimen as a reference, the most stressed region displaces farthest from the mid-point as the punch displacement increases (higher contact angle, α in Fig. 10.b). The highest stresses appear on the external surface of the sample that is the surface in contact with the electrolyte in the in-situ hydrogen charged tests.

Furthermore, when the displacement rate in the in-situ hydrogen charged tests decreases ($v_2 < v_1$ in Fig. 10.a), failure takes place at lower P_{max} and d_{max} values (lower W_{SPT} and higher embrittlement), α angle decreases as does failure diameter ϕ, as is shown in Fig. 10.c.

Fig. 11 was obtained at the end of the in-situ hydrogen charged test performed under a cathodic density current of 1.00 mA/cm^2 and a displacement rate of 0.02 mm/min. It can be seen in this figure that many cracks were initiated on the lower surface of the specimen that is in contact with the electrolyte. H.S. Shin et al. [47] concluded that these secondary cracks correspond to local hydrogen accumulations and that their position changes during the SPT test due to the change in the location of the region submitted to maximum stresses. In this case, the critical crack started growing throughout the specimen thickness at approximately 45° to the principal stress direction. This is a ductile mechanism (under maximum shear stress). However, the crack eventually deviated from this direction and final failure took finally place perpendicularly to the principal stress plane in a brittle behaviour.

5. Conclusions

The susceptibility of 42CrMo4-700 steel under different hydrogen environment conditions was qualitatively and quantitatively evaluated using in-situ electrochemical hydrogen charged SPTs performed with two different cathodic current densities and a wide range of displacement rates.

A greater susceptibility to HE was observed when the displacement rate is lower (longer testing time and more time for hydrogen diffusion) and the applied cathodic current density is higher (higher hydrogen concentration in equilibrium with the hydrogenated medium).

Hydrogen pre-charging does not modify the results obtained in the in-situ hydrogen charged SP tests. During the in-situ SPTs, the high plastic deformation generated on the surface of the specimen in contact

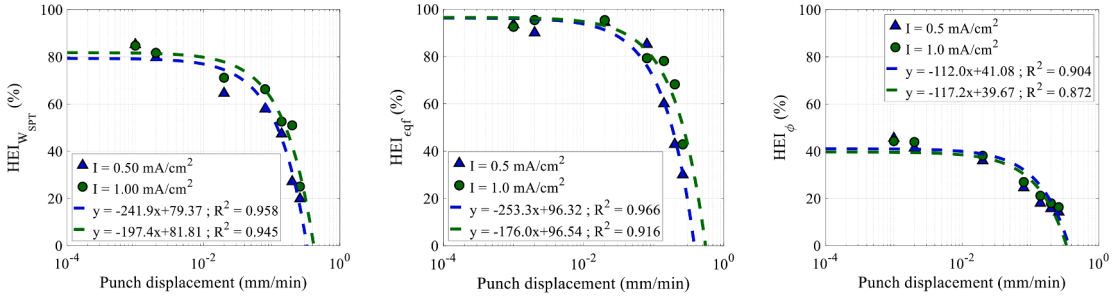

(a) *(b)* *(c)*

Fig. 9. Hydrogen embrittlement index, HEI, calculated from: (a) W_{SPT}, (b) ε_{qf}, (c) ϕ.

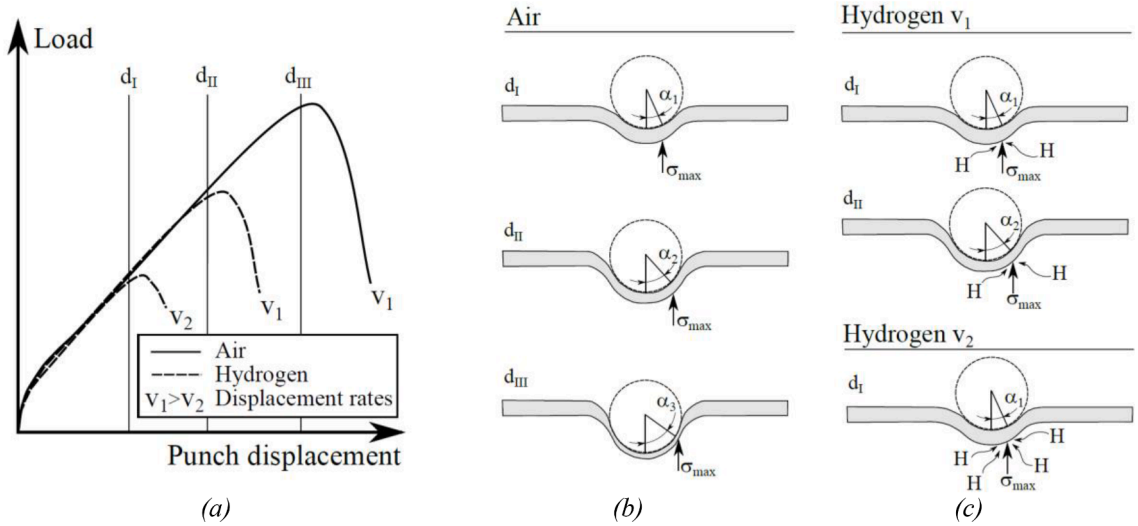

Fig. 10. Effect of SPT conditions on: (a) SPT curves, (b) location of maximum stress in SPT in air and (c) location of maximum stress in in-situ hydrogen charging SPTs at two different punch displacement rates ($v_2 < v_1$).

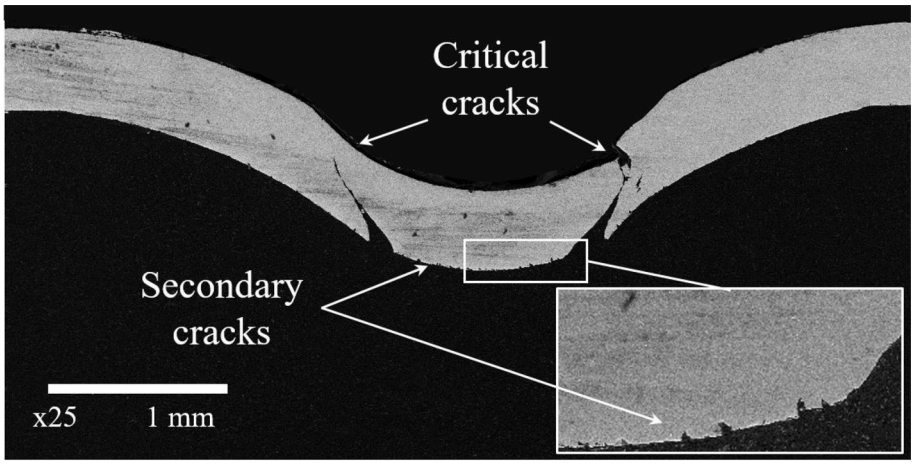

Fig. 11. SPT failed sample with a cathodic density current of 1 mA/cm^2 and a displacement rate of 0.02 mm/min.

with the electrolyte introduces a much larger quantity of hydrogen that is introduced in the pre-charge phase.

Hydrogen embrittlement was evaluated using three embrittlement indices based on three different SPTs parameters: the *fracture SPT energy (HEI_W), the equivalent biaxial deformation (HEI_{eqf})*, and *the diameter at failure (HEI_ϕ)*. All of them showed a similar trend, with a decreasing dependence on the punch displacement rate as this parameter drops, but all them finally tend towards a constant value when a critical displacement rate of 0.002 mm/min is attained. Nevertheless, since the first two indices capture the embrittlement phenomenon more accurately, both HEI_{WSPT} and HEI_{eqf} are proposed as the best indices to evaluate hydrogen embrittlement by means of in-situ hydrogen charging SPTs.

Declaration of Competing Interest

The authors declare that they have no known competing financial interests or personal relationships that could have appeared to influence the work reported in this paper.

Data availability

The data that has been used is confidential.

Acknowledgements

This work was supported by the Spanish Ministry of Science, Innovation and Universities with the project RTI2018-096070-B-C31. The author V. Arniella would like to thank this ministry the grant FPI-RTI2018-096070-B-C31. The author G. Álvarez would acknowledges the University of Oviedo for the support received with the Margarita Salas Grant (Ref.: MU-21-UP2021-030). Finally, the authors thank the Scientific and Technical Service, University of Oviedo, and Imperial College London, for the use of the SEM JEOL-JSM5600 and ZEISS Gemini – Oxford EBSD Aztec Advanced scanning electron microscopes, respectively.

References

[1] N. AbouSeada, T.M. Hatem, Climate action: Prospects of green hydrogen in Africa, Energy Rep. 8 (2022) 3873–3890, https://doi.org/10.1016/J.EGYR.2022.02.225.
[2] O. Barrera, D. Bombac, Y. Chen, T.D. Daff, E. Galindo-Nava, P. Gong, D. Haley, R. Horton, I. Katzarov, J.R. Kermode, C. Liverani, M. Stopher, F. Sweeney, Understanding and mitigating hydrogen embrittlement of steels: a review of experimental, modelling and design progress from atomistic to continuum, J. Mater. Sci. 53 (1978) 6251–6290, https://doi.org/10.1007/s10853-017-1978-5.
[3] S.K. Bonagani, B. Vishwanadh, S. Tenneti, N. Naveen Kumar, V. Kain, Influence of tempering treatments on mechanical properties and hydrogen embrittlement of 13 wt% Cr martensitic stainless steel, Int. J. Press. Vessel. Pip. 176 (2019), 103969, https://doi.org/10.1016/j.ijpvp.2019.103969.

[4] A. Zafra, G. Álvarez, J. Belzunce, J.M. Alegre, C. Rodríguez, Fracture toughness of coarse-grain heat affected zone of quenched and tempered CrMo steels with internal hydrogen: Fracture micromechanisms, Eng. Fract. Mech. 241 (2021), https://doi.org/10.1016/J.ENGFRACMECH.2020.107433.

[5] A. Zafra, G. Álvarez, J. Belzunce, C. Rodríguez, Influence of tempering time on the fracture toughness of hydrogen pre-charged 42CrMo4 steel, Theor. Appl. Fract. Mech. 117 (2022), 103197, https://doi.org/10.1016/J.TAFMEC.2021.103197.

[6] D. Hardie, E.A. Charles, A.H. Lopez, Hydrogen embrittlement of high strength pipeline steels, Corros. Sci. 48 (2006) 4378–4385, https://doi.org/10.1016/j.corsci.2006.02.011.

[7] T. Depover, D. Pérez Escobar, E. Wallaert, Z. Zermout, K. Verbeken, Effect of hydrogen charging on the mechanical properties of advanced high strength steels, Int. J. Hydrogen Energy. 39 (2014) 4647–4656, https://doi.org/10.1016/J.IJHYDENE.2013.12.190.

[8] D.K. Singh, R.K. Singh Raman, S.K. Maiti, T.K. Bhandakkar, S. Pal, Investigation of role of alloy microstructure in hydrogen-assisted fracture of AISI 4340 steel using circumferentially notched cylindrical specimens, Mater. Sci. Eng. A. 698 (2017) 191–197, https://doi.org/10.1016/J.MSEA.2017.05.056.

[9] Y. Hu, C. Dong, H. Luo, K. Xiao, P. Zhong, X. Li, Study on the Hydrogen Embrittlement of Aermet100 Using Hydrogen Permeation and SSRT Techniques, (n.d.). https://doi.org/10.1007/s11661-017-4159-x.

[10] Y.H. Fan, B. Zhang, H.L. Yi, G.S. Hao, Y.Y. Sun, J.Q. Wang, E.H. Han, W. Ke, The role of reversed austenite in hydrogen embrittlement fracture of S41500 martensitic stainless steel, Acta Mater. 139 (2017) 188–195, https://doi.org/10.1016/j.actamat.2017.08.011.

[11] H. Kyriakopoulou, P. Karmiris-Obratański, A. Tazedakis, N. Daniolos, E. Dourdounis, D. Manolakos, D. Pantelis, Investigation of hydrogen embrittlement susceptibility and fracture toughness drop after in situ hydrogen cathodic charging for an X65 pipeline steel, Micromachines. 11 (2020) 430, https://doi.org/10.3390/mi11040430.

[12] G. Álvarez, L.B. Peral, C. Rodríguez, T.E. García, F.J. Belzunce, Hydrogen embrittlement of structural steels: effect of the displacement rate on the fracture toughness of high-pressure hydrogen pre-charged samples, Int. J. Hydrogen Energy. 44 (2019), https://doi.org/10.1016/j.ijhydene.2019.03.279.

[13] L.B. Peral, A. Zafra, J. Belzunce, C. Rodríguez, Effects of hydrogen on the fracture toughness of CrMo and CrMoV steels quenched and tempered at different temperatures, Int. J. Hydrogen Energy. 44 (2019) 3953–3965, https://doi.org/10.1016/J.IJHYDENE.2018.12.084.

[14] Y. Murakami, S. Matsuoka, Effect of hydrogen on fatigue crack growth of metals, Eng. Fract. Mech. 77 (2010) 1926–1940, https://doi.org/10.1016/J.ENGFRACMECH.2010.04.012.

[15] S. Brück, V. Schippl, M. Schwarz, H.J. Christ, C.P. Fritzen, S. Weihe, Hydrogen embrittlement mechanism in fatigue behavior of austenitic and martensitic stainless steels, Metals (Basel). 8 (2018) 339, https://doi.org/10.3390/met8050339.

[16] A. Alvaro, D. Wan, V. Olden, A. Barnoush, Hydrogen enhanced fatigue crack growth rates in a ferritic Fe-3 wt%Si alloy and a X70 pipeline steel, Eng. Fract. Mech. 219 (2019), 106641, https://doi.org/10.1016/j.engfracmech.2019.106641.

[17] T.E. García, C. Rodríguez, F.J. Belzunce, I. Peñuelas, B. Arroyo, Development of a methodology to study the hydrogen embrittlement of steels by means of the small punch test, Mater. Sci. Eng. A. 626 (2015) 342–351, https://doi.org/10.1016/j.msea.2014.12.083.

[18] G. Álvarez, A. Zafra, C. Rodríguez, F.J. Belzunce, I.I. Cuesta, SPT analysis of hydrogen embrittlement in CrMoV welds, Theor. Appl. Fract. Mech. 110 (2020), 102813, https://doi.org/10.1016/j.tafmec.2020.102813.

[19] Y. Deng, A. Barnoush, Hydrogen embrittlement revealed via novel in situ fracture experiments using notched micro-cantilever specimens, Acta Mater. 142 (2018) 236–247, https://doi.org/10.1016/j.actamat.2017.09.057.

[20] UNE-EN 10371, Materiales metálicos. Método de ensayo miniatura de punzonado, 2022.

[21] T. Abt, G. Álvarez, C. Rodríguez, M.L. Maspoch, Using the small punch test to analyse the influence of ultraviolet radiation on the mechanical behaviour of recycled polyethylene terephthalate, J. Strain Anal. Eng. Des. 54 (2019), https://doi.org/10.1177/0309324719833237.

[22] C. Quintana, C. Rodríguez, F.J. Belzunce, A.C. Caballero, C. Baudín, Ceramic materials characterization using miniature mechanical tests: comparison between B3B and SPT tests, J. Eur. Ceram. Soc. (2019), https://doi.org/10.1016/J.JEURCERAMSOC.2019.06.019.

[23] C. Rodríguez, J. García Cabezas, E. Cárdenas, F.J. Belzunce, C. Betegón, Mechanical properties characterization of heat-affected zone using the small punch test, Weld. J. (Miami, Fla). 88 (2009) 188s–192s.

[24] C. Rodríguez, E. Cárdenas, F.J. Belzunce, C. Betegón, Fracture Characterization of Steels by Means of the Small Punch Test, Exp. Mech. 53 (2013) 385–392, https://doi.org/10.1007/s11340-012-9637-x.

[25] T.E. García, C. Rodríguez, F.J. Belzunce, C. Suárez, Estimation of the mechanical properties of metallic materials by means of the small punch test, J. Alloys Compd. 582 (2014) 708–717, https://doi.org/10.1016/J.JALLCOM.2013.08.009.

[26] ASTM International, Standard Test Method for Small Punch Testing of Metallic Materials. E3205-20, 2020. https://doi.org/10.1520/E3205-20.2.

[27] Asociación Española de Normalización, Materiales metálicos. Método de ensayo miniatura de punzonado, 2022. http://www.une.org.

[28] B. Arroyo, J.A. Álvarez, R. Lacalle, C. Uribe, T.E. García, C. Rodríguez, Analysis of key factors of hydrogen environmental assisted cracking evaluation by small punch test on medium and high strength steels, Mater. Sci. Eng. A. 691 (2017) 180–194, https://doi.org/10.1016/J.MSEA.2017.03.006.

[29] D. Andrés, P. Dymáček, Study of the upper die clamping conditions in the small punch test, Theor. Appl. Fract. Mech. 86 (2016) 117–123, https://doi.org/10.1016/J.TAFMEC.2016.07.012.

[30] P. Dymáček, Recent developments in small punch testing: applications at elevated temperatures, Theor. Appl. Fract. Mech. 86 (2016) 25–33, https://doi.org/10.1016/J.TAFMEC.2016.09.013.

[31] T.E. García, B. Arroyo, C. Rodríguez, F.J. Belzunce, J.A. Álvarez, Small punch test methodologies for the analysis of the hydrogen embrittlement of structural steels, Theor. Appl. Fract. Mech. 86 (2016) 89–100, https://doi.org/10.1016/J.TAFMEC.2016.09.005.

[32] B. Arroyo, J.A. Álvarez, R. Lacalle, P. González, Using Small Punch tests in environment under static load for fracture toughness estimation in hydrogen embrittlement, (n.d.).

[33] K.O. Bae, H.S. Shin, U.B. Baek, Quantitative evaluation of hydrogen embrittlement susceptibility in various steels for energy use using an in-situ small punch test, Int. J. Hydrogen Energy. 46 (2021) 20107–20118, https://doi.org/10.1016/j.ijhydene.2021.03.130.

[34] G. Álvarez, A. Zafra, F.J. Belzunce, C. Rodríguez, Effect of internal hydrogen on the fatigue crack growth rate in the coarse-grain heat-affected zone of a CrMo steel, Metals (Basel). 12 (2022), https://doi.org/10.3390/met12040673.

[35] T. Zhang, W. Zhao, Y. Zhao, K. Ouyang, Q. Deng, Y. Wang, W. Jiang, Effects of surface oxide films on hydrogen permeation and susceptibility to embrittlement of X80 steel under hydrogen atmosphere, Int. J. Hydrogen Energy. 43 (2018) 3353–3365, https://doi.org/10.1016/J.IJHYDENE.2017.12.170.

[36] N.E. Nanninga, Y.S. Levy, E.S. Drexler, R.T. Condon, A.E. Stevenson, A.J. Slifka, Comparison of hydrogen embrittlement in three pipeline steels in high pressure gaseous hydrogen environments, Corros. Sci. 59 (2012) 1–9, https://doi.org/10.1016/j.corsci.2012.01.028.

[37] W. Zhao, T. Zhang, Z. He, J. Sun, Y. Wang, Determination of the Critical Plastic Strain-Induced Stress of X80 Steel through an Electrochemical Hydrogen Permeation Method, Electrochim. Acta. 214 (2016) 336–344, https://doi.org/10.1016/J.ELECTACTA.2016.08.026.

[38] D. Pérez Escobar, T. Depover, E. Wallaert, L. Duprez, M. Verhaege, K. Verbeken, Thermal desorption spectroscopy study of the interaction between hydrogen and different microstructural constituents in lab cast Fe–C alloys, Corros. Sci. 65 (2012) 199–208, https://doi.org/10.1016/J.CORSCI.2012.08.017.

[39] A. Zafra, J. Belzunce, C. Rodríguez, Hydrogen diffusion and trapping in 42CrMo4 quenched and tempered steel: influence of quenching temperature and plastic deformation, Mater. Chem. Phys. 255 (2020), 123599, https://doi.org/10.1016/j.matchemphys.2020.123599.

[40] A. Zafra, L.B. Peral, J. Belzunce, C. Rodríguez, Effect of hydrogen on the tensile properties of 42CrMo4 steel quenched and tempered at different temperatures, Int. J. Hydrogen Energy. (2018), https://doi.org/10.1016/j.ijhydene.2018.03.158.

[41] A. Zafra, L.B. Peral, J. Belzunce, C. Rodríguez, Effects of hydrogen on the fracture toughness of 42CrMo4 steel quenched and tempered at different temperatures, Int. J. Press. Vessel. Pip. 171 (2019) 34–50, https://doi.org/10.1016/J.IJPVP.2019.01.020.

[42] UNE-EN 1002-1, Materiales metálicos Ensayo de tracción Parte 1 : Método de ensayo a temperatura ambiente, (2017).

[43] ASTM E 1820-01: Standard Test Method for Measurement of Fracture Toughness, 2001. https://doi.org/10.1520/E1820-09.2.

[44] G. Álvarez, A. Zafra, F.J. Belzunce, C. Rodríguez, Hydrogen embrittlement analysis in a CrMoV steel by means of sent specimens, Theor. Appl. Fract. Mech. 106 (2020), 102450, https://doi.org/10.1016/J.TAFMEC.2019.102450.

[45] V. Arniella, A. Zafra, G. Álvarez, J. Belzunce, C. Rodríguez, Comparative study of embrittlement of quenched and tempered steels in hydrogen environments, Int. J. Hydrogen Energy. (2022), https://doi.org/10.1016/J.IJHYDENE.2022.03.203.

[46] G. Álvarez, C. Rodríguez, F.J. Belzunce, T.E. García, Use of notched small punch test specimens for the determination of fracture properties in structural steels, Theor. Appl. Fract. Mech. 106 (2020), https://doi.org/10.1016/j.tafmec.2019.102442.

[47] H.S. Shin, K.O. Bae, U.B. Baek, S.H. Nahm, Establishment of an in-situ small punch test method for characterizing hydrogen embrittlement behaviors under hydrogen gas environments and new influencing factor, Int. J. Hydrogen Energy. 44 (2019) 23472–23483, https://doi.org/10.1016/J.IJHYDENE.2019.07.029.

[48] H.S. Shin, N.A. Custodio, U.B. Baek, Numerical analysis for characterizing hydrogen embrittlement behaviors induced in STS316L stainless steel using an in-situ small-punch test, Theor. Appl. Fract. Mech. 116 (2021), 103139, https://doi.org/10.1016/J.TAFMEC.2021.103139.